On the Miniaturization of Semi-Planar Chiral Metamaterial Structures

Davoud Zarifi, Mohammad Soleimani, Vahid Nayyeri, *Student Member, IEEE*, and Jalil Rashed-Mohassel, *Senior Member, IEEE*

***Abstract*—In this paper, miniaturized chiral metamaterial (CMM) structures with smaller unit cells or lower resonant frequencies are investigated. In achieving this purpose, three general ideas are proposed: using dendritic fractal geometry, using some wideband antenna designs, and utilizing echelon meandered structures. Based on these methods, some miniaturized CMM structures with giant optical activity and negative refraction indices are proposed for the right and left circularly polarized waves and their effective parameters are retrieved. The proposed structures possess smaller unit cell sizes and some of them exhibit considerable optical activity compared with similar CMM designs; thus, they can be used as ultrathin microwave polarization rotators.**

***Index Terms*—Chiral metamaterials, miniaturization, optical activity, negative refractive index, dendritic fractal geometry, wideband antenna designs, echelon meandered geometries.**

I. Introduction

RECENTLY, chiral metamaterials have attracted increasing attention because of their interesting and unique properties such as giant optical activity and negative refraction. In fact, CMMs are metamaterials (MTMs) made of unit cells without any mirror symmetry. This property results in the breaking degeneracy of two circularly polarized waves, i.e. right circularly polarized (RCP) and left-circularly polarized (LCP) waves with different refractive indices. For a time harmonic field with *exp*(*-iωt*) convention, chiral media are characterized by the following constitutive relations [1]:

$$\begin{pmatrix}\mathbf{D}\\ \mathbf{B}\end{pmatrix}=\begin{pmatrix}\varepsilon_0\varepsilon & i\kappa/c\\ -i\kappa/c & \mu_0\mu\end{pmatrix}\begin{pmatrix}\mathbf{E}\\ \mathbf{H}\end{pmatrix}, \tag{1}$$

where ε, μ, c and κ are the relative permittivity, relative permeability, speed of light in free space, and the chirality parameter, respectively. Using Maxwell's equations the wave equation can be derived for an electromagnetic wave propagating in an isotropic and homogeneous chiral media given by:

$$\nabla^2\mathbf{E}+2\frac{\kappa\omega}{c_0}\nabla\times\mathbf{E}+\frac{\omega^2}{c_0^2}(\mu\varepsilon-\kappa^2)\mathbf{E}=0. \tag{2}$$

It can be seen that linearly polarized waves cannot be polarization eigen-states of this wave equation. Assuming all fields to be plane waves and using the wavefield decomposition, it is observed that there are two eigen-modes in a chiral medium: right circularly polarized (RCP) wave (+) and left circularly polarized (LCP) wave (-). The refractive indices for the RCP and LCP waves are given by [1]:

$$n_{\pm}=n\pm\kappa \tag{3}$$

where $n=\sqrt{\varepsilon\mu}$. Both RCP and LCP waves have the same impedance given by $z/z_0=\sqrt{\mu/\varepsilon}$ where z_0 is the impedance of the free space. Given a large enough chirality, the negativity of n_+ or n_- is possible [2]. In fact, negative refraction can be realized in CMMs with a strong chirality, with neither negative permittivity nor permeability required. Based on this concept, several multi-layered structures with four-fold rotational symmetry such as twisted rosettes [3], twisted crosses [4], twisted U-SRRs [5], double-layer CMM structure [6], conjugated gammadion [7], complementary CMM structure [8], and a dual-band CMM structure [9] have been suggested as the kinds of semi-planar CMM structures. In order to obtain a pure optical activity, both chiral symmetry (lack of any mirror symmetry) and four-fold rotational symmetry are present in the unit cells of these CMM designs. In recent years, several other applications have been proposed for chiral metamaterials such as realizing structures with strong optical activity [10-12], realizing negative refraction index in Terahertz regime [13-15], circular polarizers [16, 17], wide angle and polarization independent microwave absorbers [18], gain enhancement and axial ratio (AR) improvement of circularly polarized antennas [19].

The parameter retrieval of electromagnetic parameters of semi-planar CMM structures is generally the same as regular MTMs. However, due to the chiral nature of medium and different interactions among its chiral particles and RCP and

Manuscript received October 00, 0000; revised January 0, 0000; accepted September 00, 0000. Date of publication September 00, 0000; date of current version September 00, 0000.

D. Zarifi, M. Soleimani, and V. Nayyeri are with the Antenna and Microwave Research Laboratory, School of Electrical Engineering, Iran University of Science and Technology (IUST), Tehran, Iran (email: zarifi@iust.ac.ir; soleimani@iust.ac.ir; nayyeri@iust.ac.ir).

J. Rashed-Mohassel is with the Center of Excellence on Applied Electromagnetic Systems, School of ECE, University of Tehran, Tehran, Iran, (e-mail: jrashed@ut.ac.ir).

Color versions of one or more of the figures in this paper are available online at http:// ieeexplorer.ieee.org

LCP waves, it is somewhat more complicated. In fact, the circularly polarized transmission coefficients ($T_{\pm}$), and reflection coefficients ($R_{\pm}$) of RCP and LCP waves should be measured. For simplicity, a linearly polarized EM wave (first, electric field in the x and then in the y direction) is incident on the CMM structure and the linear transmission coefficients, T_{xx}, T_{yx} , T_{yy}, and T_{xy}, and the linear reflections, R_{xx}, R_{yx} , R_{yy}, and R_{xy}, are measured. Here, the first subscript indicates the transmitted (reflected) field polarization (x- or y-polarized), and the second indicates the incident field polarization. Then, the linearly polarized transmissions and reflections should be converted to circular transmission coefficients (T_{++}, T_{+-}, T_{-+}, T_{--}) and reflection coefficients (R_{++}, R_{+-}, R_{-+}, R_{--}), where the first subscript indicates the transmitted (reflected) field polarization (RCP or LCP), and the second indicates the incident field polarization. It can be easily shown that the circular scattering coefficients are converted from the linear scattering coefficients using the following equation [19, 20]:

$$\begin{pmatrix} T_{++} & T_{+-} \\ T_{-+} & T_{--} \end{pmatrix} = \frac{1}{2}\begin{pmatrix} (T_{xx}+T_{yy})-j(T_{xy}-T_{yx}) & (T_{xx}-T_{yy})+j(T_{xy}+T_{yx}) \\ (T_{xx}-T_{yy})-j(T_{xy}+T_{yx}) & (T_{xx}+T_{yy})+j(T_{xy}-T_{yx}) \end{pmatrix}, \quad (4)$$

where, T can also be replaced with R. Once z, κ and $n_{\pm}$ were unambiguously determined using a standard parameter retrieval method [21], other effective parameters of the CMM structure can be identified subsequently, $n = (n_{+}+ n_{-})/2$, $\varepsilon = n/z$ and $\mu = nz$. The difference between the amplitudes (circular dichroism) and phases (optical activity) of RCP and LCP transmission coefficients are characterized by ellipticity

$$\eta = \arctan\left(\frac{|T_{++}|-|T_{--}|}{|T_{++}|+|T_{--}|}\right) \quad (5)$$

and polarization azimuth rotation

$$\theta = \frac{1}{2}\left[\arg(T_{++})-\arg(T_{--})\right] \quad (6)$$

respectively [4, 22].

The semi-planar CMM structures proposed recently, exhibit significant optical activity and negative refractive index for circular polarizations at parts of 4-8 GHz frequency band, when the transverse dimensions of their unit cells are 15×15 mm^2 or 10×10 mm^2. Also, such structures can be scaled to other frequencies. The purpose of this paper is to propose miniaturized CMM structures with smaller unit cells or lower resonant frequencies in order to reduce Bragg scattering and Wood anomalies [23] and also decrease fabrication costs. Based on the mechanism of resonances in CMM structures, three general ideas to miniaturize CMMs are proposed include using fractal geometries, wideband antenna designs, and meandered structures.

A significant application of miniaturized CMM structures is in the circularly polarized antennas. From the practical point of view, the significant influence of semi-planar CMM structures on the important characteristics of circularly polarized antennas has been recently investigated [19]. It is clear that the retrieved electromagnetic parameters of CMM structures are only valid for a rather large array consisting of many unit cells, while the sizes of antenna and its cover are finite. To rectify this problem and achieve smaller covers, the miniaturized CMM structures having smaller unit cells can be utilized.

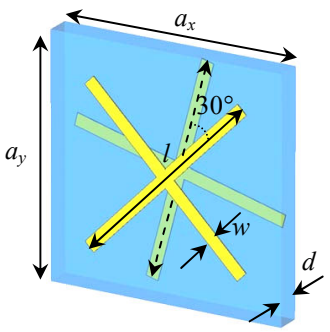

Fig. 1. Unit cell of twisted crosses structure [4]. The geometric parameters are given by $a_x = a_y = 15$ *mm*, $l = 14$ *mm*, $w = 0.7$ *mm* and $d = 1.6$ *mm*.

The organization of this paper is as follows: in Sec. II, the miniaturized CMM structures based on dendritic fractal geometry are proposed. In Sec. III application of the wideband antenna designs in miniaturizing CMMs is introduced. In Sec. IV miniaturized CMMs based on meandered structured are proposed. Finally, summary and conclusions are provided in Sec. V.

II. Miniaturized CMM Structures Based On The Dendritic Fractal Geometry

The bilayer cross-wires or twisted crosses design is an example of semi-planar CMM structures that have been already published [4]. The unit cell of this structure constructed by two cross-wires patterned on the opposite sides of an FR-4 board with the dielectric constant of 4.5, dielectric loss tangent of 0.025, and the thickness of 1.6 mm as shown in Fig. 1. The investigation of behavior of this structure around resonance frequencies shows that its optical activity and negative refractive indices can be attributed to the interaction of magnetic and electric dipole moments. Therefore, it is expected that the resonant frequencies of the structure drop as the length of cross-wires is increased. One type of simple fractal geometry that can be utilized to increase the length of wires is a dendritic fractal structure. This fractal is generated by an iterative sequence to the starting simple wire structure. In the first iteration, the top segment of this wire is split at an almost optimized angle, θ = 60°. As the iterative process continues, the end segment of each branch splits into two branches as shown in Figs. 2(a) and (e). The lengths of straight sections in the first four iterations are given by $l/2$, $l/2$; $l/2$, $l/4$, $l/4$; $l/2$, $l/4$, $l/8$, $l/8$; $l/2$, $l/4$, $l/8$, $l/16$, $l/16$. It can be easily seen that after the *n-th* iteration, the total electrical length of wire equals:

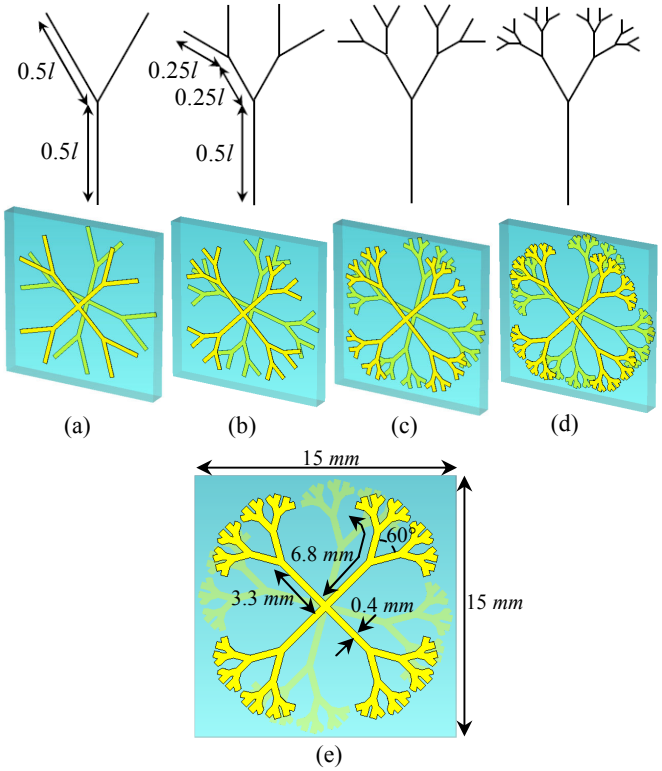

Fig. 2. (a) – (d) The first fourth iterations of dendritic fractal geometry and corresponding unit cell of CMM structures. (e) Top view of the unit cell of the fourth iteration of dendritic CMM structure. The geometric parameters are shown.

$$\begin{cases} l_n = 0.5l + l_{n-1}, & n \geq 1 \\ l_0 = l \end{cases} . \tag{7}$$

So, after the fourth iteration the total electrical length of wire equals 3*l*. It should be noticed that, due to the physical constraints, higher iterations cannot be utilized; however the miniaturization benefits are achieved in the first several iterations.

Also, the corresponding CMM structures are illustrated in Figs. 2(a) - (d). For instance, the unit cell parameters of the fourth iteration dendritic fractal CMM structure are shown in Fig. 2(e). Numerical simulations are performed at the frequency range of 2 to 12 GHz using the unit cell template and frequency domain solver of CST Microwave Studio which uses a finite element method for determining transmissions and reflections. The present simulations show that for the twisted angle of 30°, performance of the proposed structures is the best. Figures 3(a) and 3(b) demonstrate the simulation results of RCP and LCP transmission coefficients of the starting structure and the first four iterations of the dendritic fractal. It can be clearly seen that the resonant frequencies of the proposed structure decrease as the number of iterations increased.

Using a standard parameter retrieval method [21], the effective parameters of the fourth iteration dendritic fractal CMM structure are retrieved and presented in Fig. 4. It is seen that after four iterations the resonant frequencies of the

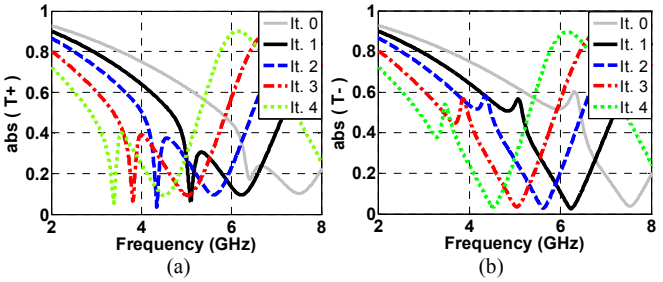

Fig. 3. Simulation results of the transmission spectra for the RCP (a) and LCP (b) waves for the first fourth iterations of the dendritic fractal CMM structure.

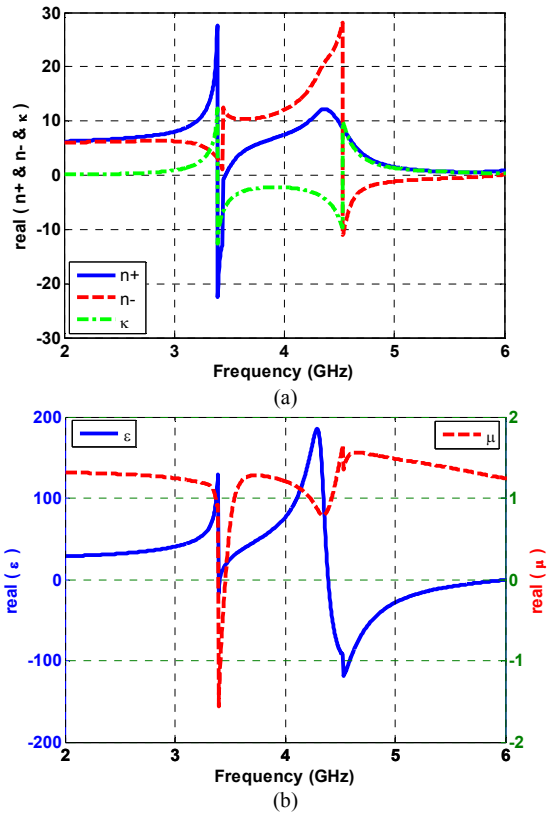

Fig. 4. The retrieved effective parameters of the fourth iteration dendritic fractal CMM structure. (a) the real parts of the RCP and LCP refractive indices and the chirality parameter. (b) the real parts of the permittivity and permeability.

proposed structure change from 6.4 GHz and 7.5 GHz to 3.4 GHz and 4.5 GHz, respectively. These drops in resonant frequencies are significant, since in order to achieve these resonant frequencies using the ordinary cross-wires, the transverse dimensions of the structure should be almost doubled. As shown in Fig. 4(a), near the resonant frequencies of 3.4 GHz and 4.5 GHz, the strong chirality parameter κ, pushes the refractive indices from positive to negative for the RCP and LCP waves, respectively. Figure 4(b) proves that the negative RCP and LCP refractive indices are due to the chiral nature of metamaterial and, not because of the simultaneous negative permittivity and permeability. For the RCP (LCP) wave, the Figure of Merit (FoM), i.e. |Re (n) / Im (n)|, is around 1.4 (0.7) at 3.4 GHz (4.5 GHz). The relatively low

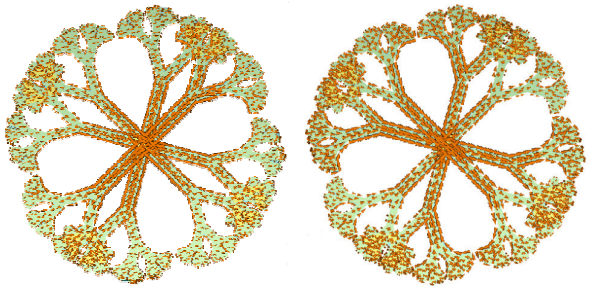

(a): RCP 3.4 GHz (b): LCP 4.5GHz

Fig. 5. The surface current distribution of the fourth iteration dendritic fractal CMM structure. (a) for the RCP wave at 3.4 GHz. (b) for the LCP wave at 4.5 GHz.

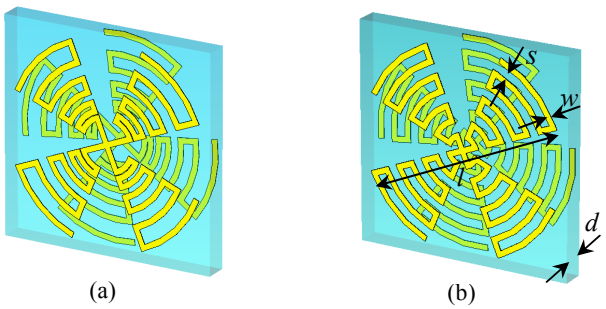

(a) (b)

Fig. 6. (a) Unit cell of log-periodic multi-turns cross wires CMM structure. (b) Unit cell of multi-turn cross wires CMM structure The geometric parameters are given by $a_x = a_y = 15$ *mm*, $l = 14.4$ *mm*, $w = 0.4$ *mm* and $s = 0.6$ *mm*, $d = 1.6$ *mm*.

FoM compared with ordinary well-known MTMs [24] which limits applicable frequency bands of negative refractive indices is mainly due to the high loss of dielectric board. Thus, the FoM and applicable frequency bands of negative refractive indices can be substantially improved using a substrate with lower loss dielectric.

The current density distributions of the proposed structure at magnetic and electric resonant frequencies are shown in Fig. 5. At the magnetic resonant frequency of 3.4 GHz, two couples of anti-parallel currents flow on the opposite sides of the board and simulating two current loops and an asymmetric resonant mode, at the electric resonant frequency of 4.5 GHz, two couples of parallel currents, simulate an electric dipole and a symmetric resonant mode.

The proposed miniaturized CMM structure can be scaled to other frequencies. For instance, numerical simulations show that with planar scaling of the structure with a factor of 0.6, the resonant frequencies change from 3.4 GHz and 4.5 GHz to 5.9 GHz (3.4/0.58) and 6.5 GHz (4.5/0.6), respectively.

III. Miniaturized CMM Structures Based On The Wideband Antenna Designs

As mentioned in the previous section, the performance of semi-planar CMM structures is based on the coupling of the electric or magnetic dipoles created on the opposite sides of the dielectric board. Since increasing the electrical length of these dipoles resulted in dropping the resonant frequencies, the wideband dipole antenna designs can be used [25] instead of ordinary dipoles. This is due to the fact that the effective electrical length of the dipole increases considerably using common types of antennas such as bow-tie antenna, log-periodic toothed antenna, log-periodic wire antenna and multi-arm spiral antenna. In this section, some miniaturized CMM structures based on the log-periodic wire antenna and the four-arm square spiral antenna are proposed. Also, it should be noticed that, in this application, the log-periodic property of the antenna is not required.

A. The Multi-turns Cross-wires Structure

The unit cell of the proposed CMM structure based on the log-periodic wire antenna design is shown in Fig. 6 (a). The present simulations show that the log-periodic property does not significantly affect the performance of the structure and

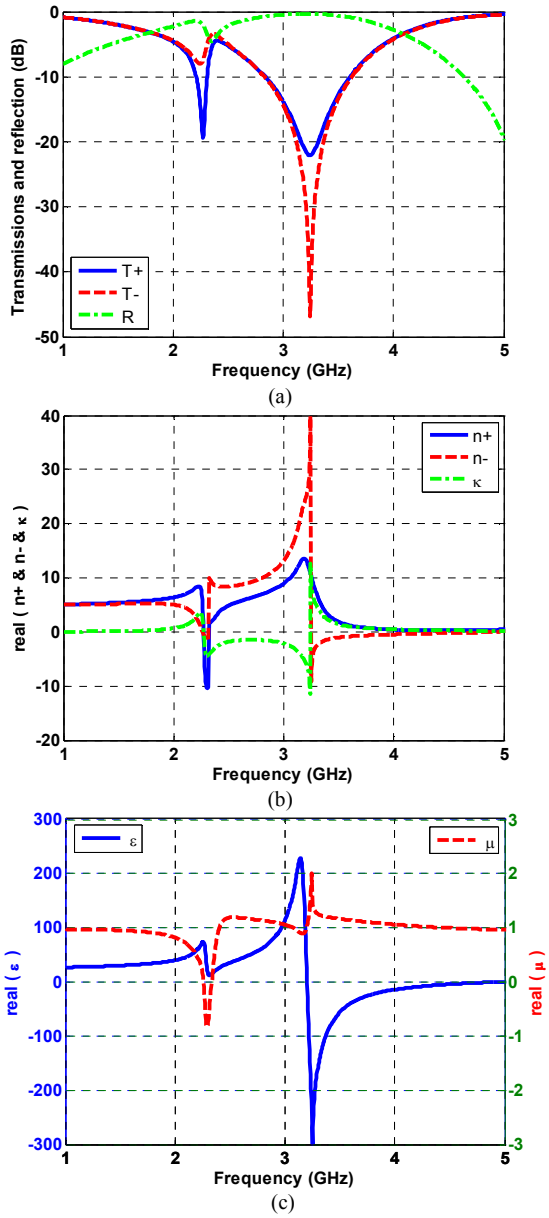

Fig. 7. (a) Simulation results of the transmissions and reflection spectra for the RCP and LCP waves for the multi-turns cross wires CMM structure. (b) the real parts of the RCP and LCP refractive indices and the chirality parameter. (c) the real parts of the effective permittivity and permeability.

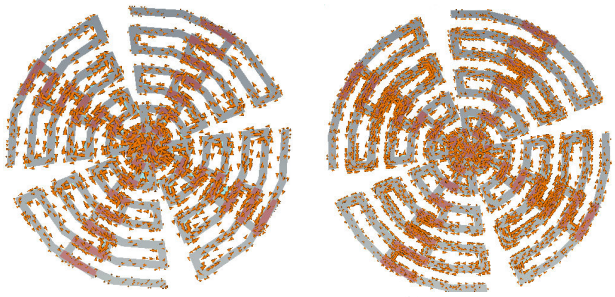

(a): RCP 2.25 GHz (b): LCP 3.3 GHZ

Fig. 8. The surface current distribution of multi-turns cross wires CMM structure. (a) for the RCP wave at 2.25 GHz. (b) for the LCP wave at 3.3 GHz.

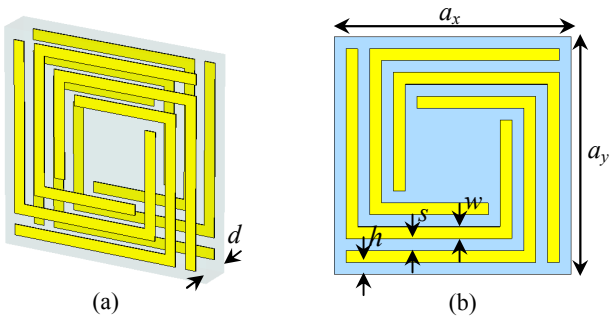

(a) (b)

Fig. 9. Unit cell of nested U-shaped CMM structure. The geometric parameters are given by $a_x = a_y = 10$ *mm*, $d = 1.6$ *mm*, $w = s = h = 0.5$ *mm*.

can be omitted. The unit cell of simplified structure is shown in Fig. 6(b). The twisted angle between the crosses on the opposite sides of the board, and the central angle of each arms are 30° and 45°, respectively, so that the chirality parameter and the electrical length of crosses could be maximized without contacting adjacent arms. The manifest characteristic of this structure is flexibility; the resonant frequencies can be adjusted by changing the turns of the arms. The proposed structure has 7 turns in each arm.

Numerical simulations are executed in a frequency range of 1 GHz to 10 GHz, and the simulated transmission and reflection spectra for the RCP and LCP waves are shown in Fig. 7(a). It should be noticed that the RCP and LCP reflection coefficients are equal [21]. It can be also observed that the resonant frequencies of this structure decrease to 2.3 GHz and 3.25 GHz; thus, the performance of this design is considerably better than that of the dendritic fractal design. In the first resonant frequency of 2.3 GHz, the transmission of RCP wave is about 12-13 dB lower than that of LCP wave while, in the second one at 3.25 GHz, the transmission of RCP wave is about 25 dB higher than that of LCP wave. Further studies indicate that the difference between the RCP and LCP transmission spectra is due to different losses as RCP and LCP waves pass the proposed CMM structure. The effective parameters of the structure are also retrieved, as presented in Figs. 7(b) and 7(c). The surface current distribution shown in Fig. 8 shows the anti-parallel and parallel currents on the top and bottom layer suggesting that the structure acts as a magnetic and electric dipole in the first and second resonant frequencies. This resonance behavior is also reflected by the effective permeability and permeability as shown in Fig. 7(c).

B. The CMM Design Using the Four-Arm Spiral Structure

The twisted U-SRRs design is one of the uniaxial CMM structures which has been recently introduced. The unit cell of this structure as shown in Fig. 9(a) is constructed by double-layered four "U" split ring resonators mutually rotated by 90° and printed on the opposite sides of an FR-4 board. This design with a 15×15 mm^2 unit cell has two resonant frequencies at 5.1 GHz and 6.4 GHz. Figure 9(b) shows the schematic diagram of one unit cell of the proposed CMM structure with the transverse dimension of 10×10 mm^2 constructed by four nested U-shaped resonator patterned on the opposite sides of the board.

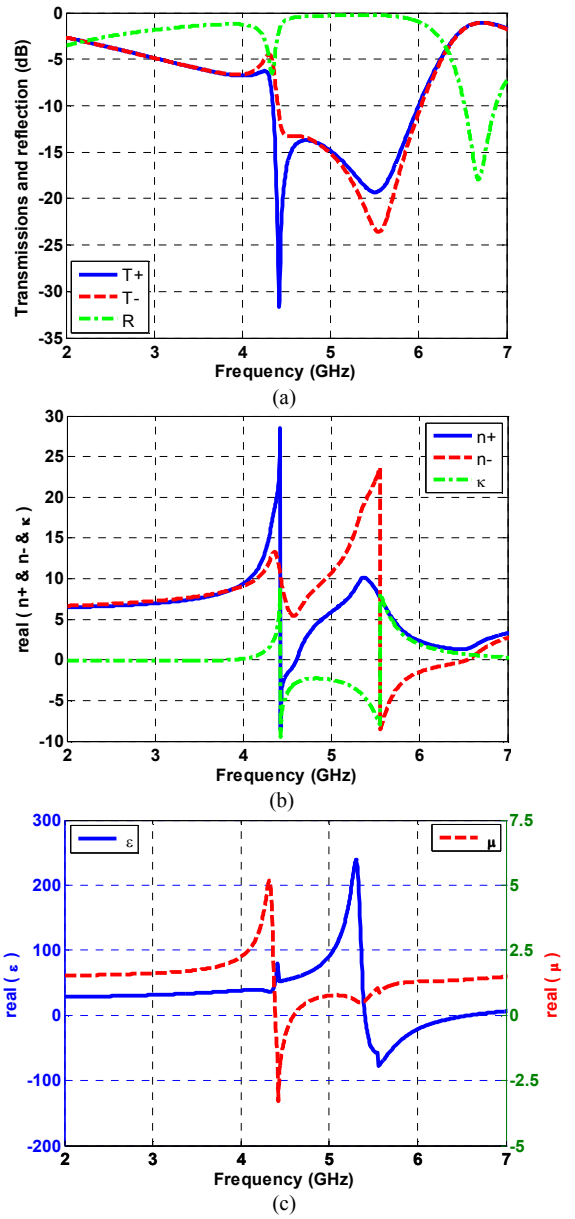

Fig. 10. (a) Simulation results of the transmissions and reflection spectra for the RCP and LCP waves for the nested U-shaped CMM structure. (b) the real parts of the RCP and LCP refractive indices and the chirality parameter. (c) the real parts of the effective permittivity and permeability.

The simulated circular transmissions and reflection in addition to the retrieved effective parameters are presented in

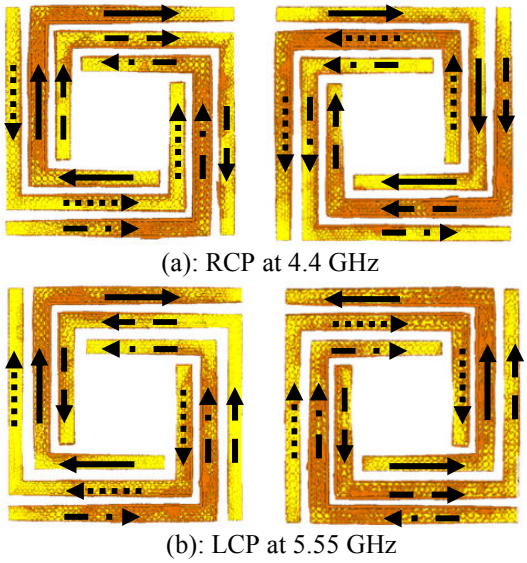

Fig. 11. The surface current distribution on the top and bottom patterns of the four-arm spiral CMM structure. (a) for the RCP wave at 4.4 GHz. (b) for the LCP wave at 5.55 GHz.

Fig. 10. According to this figure, two resonance dips at the frequencies of 4.4 GHz and 5.55 GHz are observed in both RCP and LCP transmissions, which are magnetic and electric, respectively. For the RCP (LCP) wave, the figure of merit (FoM) is around 0.8 (0.7) at 3.4 GHz (4.5 GHz). The low FoM compared with the conventional MTMs is due to the high loss dielectric board.

In order to understand the mechanism of the resonances for the nested U-shaped CMM structure, we investigate the surface current distribution on the top and bottom layers shown in Fig. 11. Figure 11(a) shows that at the resonant frequency of 4.4 GHz, four pair U-shaped resonator can be considered on the top and bottom layers. These pairs are indicated by similar arrows which denote the surface current directions. It can be seen that the corresponding U-shaped resonators act like a current loop and caused a magnetic resonance which is consistent with the permeability curve. Similarly, Fig. 11(b) shows that, at the second resonant frequency, four pair U-shaped resonators can be considered on the top and bottom layers, two pairs of which act like an electric dipole and two pairs act like a current loop; but, due to the majority simulated electric dipoles, an overall electric resonance occurs which is also reflected from the permittivity.

By completing the nested U-shaped CMM structure, a structure similar to the four-arm square spiral antenna is achieved. The simulations show that the overall behavior of this structure is similar to the prior one; however, due to the proximity of the electric and magnetic resonant frequencies, the chirality parameter in the middle of two resonances is increased. Therefore, a very significant optical activity is achieved. For instance, a CMM structure with the unit cell shown in Fig. 12 is simulated. Also, the polarization azimuth rotation angle and ellipticity angle of the transmitted wave are shown in Fig. 13. The ellipticity $\eta = 0$ corresponds to a pure optical activity effect, i.e., for the linearly polarized incident wave, the transmitted wave is linearly polarized just with the

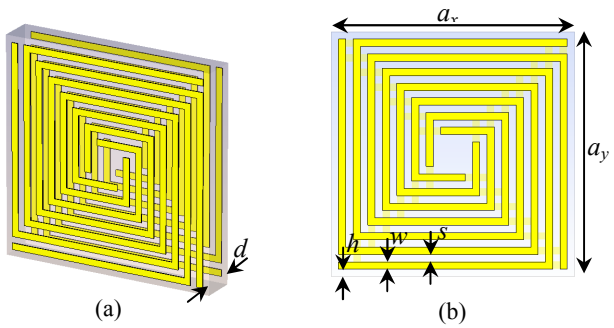

Fig. 12. Unit cell of four-arm spiral CMM structure. The geometric parameters are given by $a_x = a_y = 10$ *mm*, $d = 1.6$ *mm*, $w = s = h = 0.3$ *mm*.

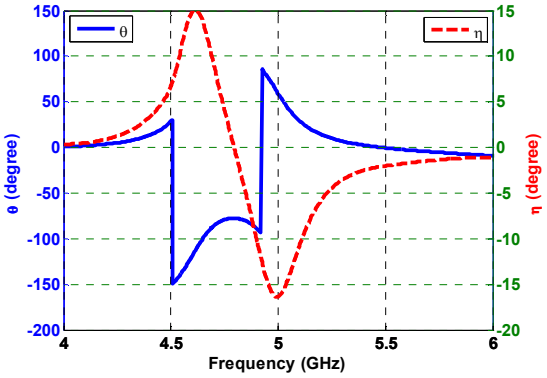

Fig. 13. The polarization azimuth rotation angle θ and the ellipticity angle η of the four-arm spiral CMM structure.

rotated angle of θ. It can be clearly seen that, at $\eta = 0$ (i.e. around the frequency of 4.8 GHz), the polarization rotation angle is around 77° for 1.6-mm-thick CMM (i.e. the rotation angle is around 3008°/λ). Thus, the proposed CMM structure possesses greater pure polarization azimuth rotation angle compared with other reported similar CMMs (e.g. the U-shaped SRRs structure [5]: 26° at 5.5 GHz and conjugated gammadions structure [7]: 30° at 6.55 GHz).

The anisotropic medium is one kind of the birefringent media which has two linearly polarized characteristic waves with different velocities, so it has been used in polarization transformation [26]. However, an anisotropic polarizer has two different intrinsic impedances; therefore, matching both impedances simultaneously is very difficult. Thus, anti-reflection layers are coated on surfaces of the polarizer to decrease mismatch. These layers can reduce reflection efficiently but the polarizer would become larger and many coated processes would be needed [27]. Recently, MTMs have been proposed to manipulate the polarization states of electromagnetic waves [28, 29]. The near complete cross polarization conversion obtained through these MTMs, which are anisotropic, is sensitive to the polarization azimuth of the incident wave. An alternative approach for the polarization conversion is done using CMMs. Meanwhile, the proposed CMM structure can be used as an ultrathin polarizer.

IV. Miniaturized CMM Structures Based On The Meandered Designs

In recent years, the meandered geometries have been used to

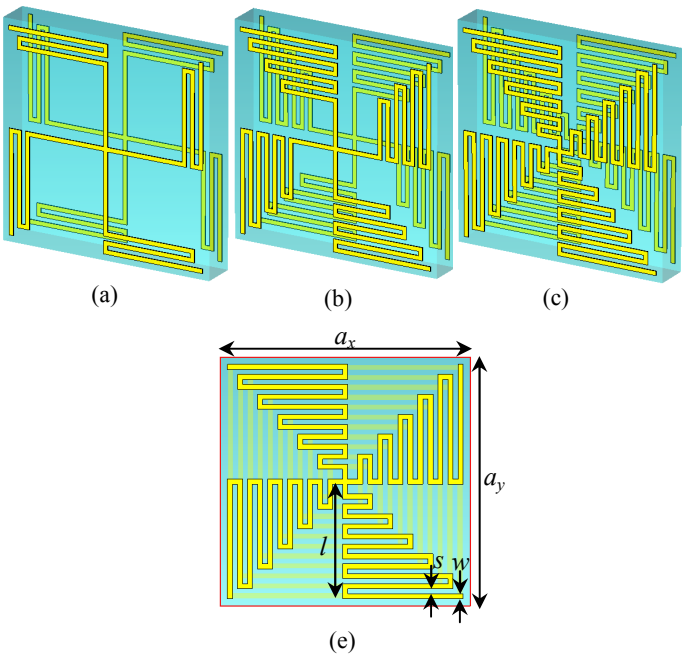

Fig. 14. (a) – (c) Unit cells of the echelon meandered conjugated gammadion CMM structures with different number of steps; Structures 1, 2, and 3, respectively. (d) Top view of the unit cell of the echelon meandered conjugated gammadion CMM structure. The geometric parameters are given by $a_x = a_y = 5$ *mm*, $l = 2.3$ *mm*, $w = s = 0.1$ *mm*.

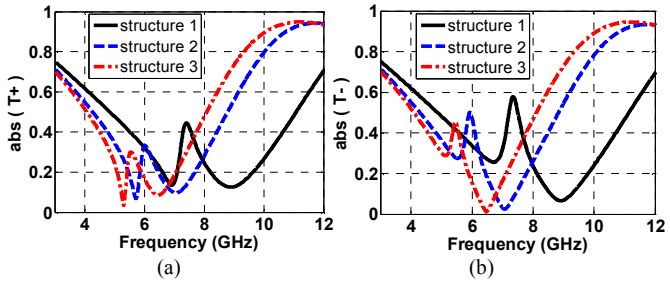

Fig. 15. Simulation results of the transmission spectra for the RCP (a) and LCP (b) waves for the echelon meandered conjugated gammadion CMM structures with different number of steps.

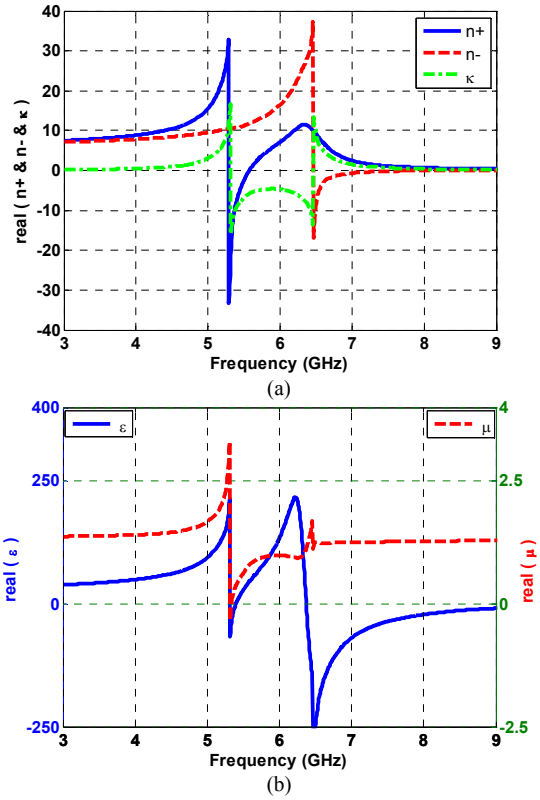

Fig. 16. The retrieved effective parameters of the echelon meandered conjugated gammadion CMM structure. (a) the real parts of the RCP and LCP refractive indices and the chirality parameter. (b) the real parts of the permittivity and permeability.

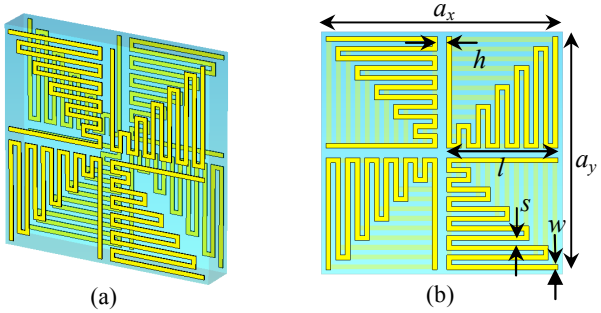

Fig. 17. (a) Unit cell of echelon meandered U-SRRs CMM structure. (b) Top view of the unit cell. The geometric parameters are given by $a_x = a_y = 10$ *mm*, $l = 4.6$ *mm*, $h = 0.4$ *mm*, $w = s = 0.2$ *mm*.

miniaturize antennas [30], microwave resonators [31], and filters [32]. In this section, two miniaturized CMM structures are proposed based on the meandered designs. In fact, these structures are the modified versions of conjugated gammadion and U-SRRs structures.

The unit cell of the first type of the proposed CMM based on meandered geometry with different numbers of steps shown in Figs. 14(a)-(c) is constructed by the echelon meandered conjugated gammadions patterned on the opposite sides of an FR-4 dielectric board ($\varepsilon_r = 4.2$ and loss tangent of 0.02) with the thickness of 0.8 mm. The echelon property of the meandered geometry, assures strong chirality of the CMM structure.

Numerical simulations are performed at the frequency range of 3 GHz to 9 GHz and circular transmissions and reflection coefficients of three structures illustrated in Fig. 14 are presented in Fig. 15. It can be clearly seen that the resonant frequencies of the proposed structures drop as the number of steps increases. Thus, as an advantage of the proposed miniaturized design, the structure is flexible so that, with changing the number of steps of the meandered structure, it is possible to design structures with other resonant frequencies. The retrieved effective parameters of the final structure (3) are shown in Fig. 16.

The ordinary conjugated gammadion CMM with a 10×10 mm^2 unit cell exhibits two resonances at 5.6 GHz and 7.85 GHz, while our proposed structure with 5×5 mm^2 unit cell have two resonances at 5.3 and 6.4 GHz.

The unit cell of the second proposed CMM based on meandered geometry is shown in Fig. 17. This design is the modified type of the U-SRRs CMM structure based on the echelon meandered geometry, that with a smaller unit cell

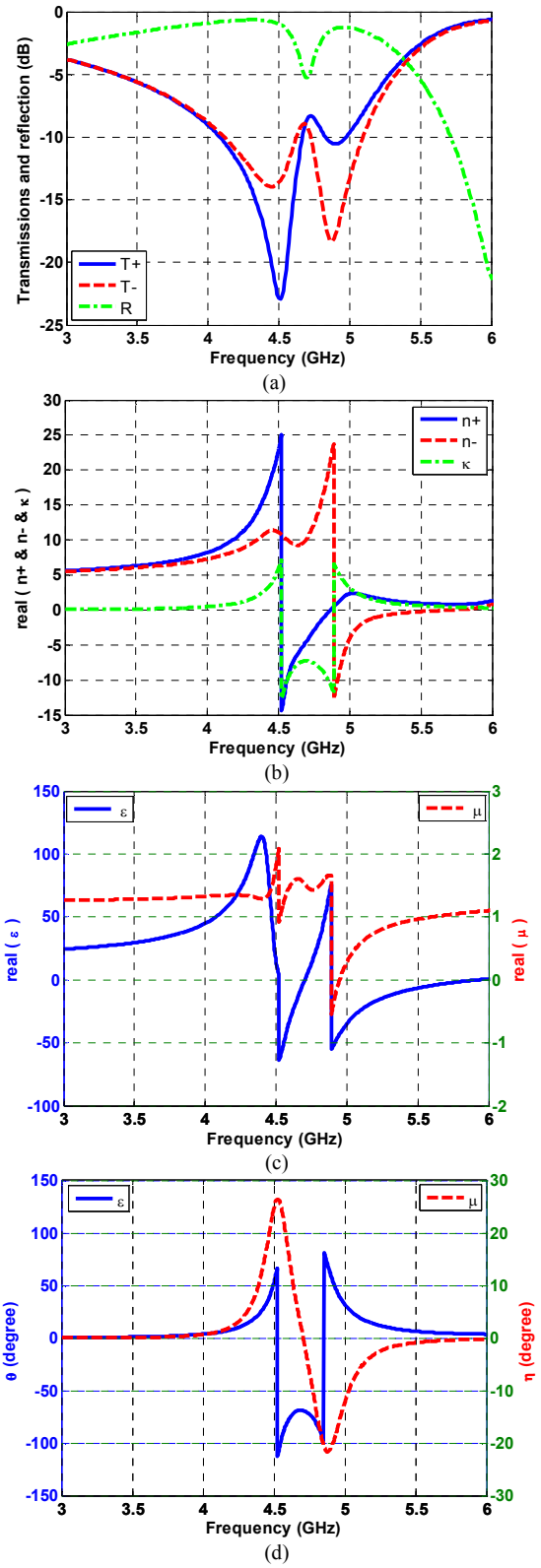

Fig. 18. (a) Simulation results of the transmissions and reflection spectra for the RCP and LCP waves. (b) the real parts of the RCP and LCP refractive indices and the chirality parameter of the echelon meandered U-SRRs CMM structure. (c) the real parts of the effective permittivity and permeability. (d) the polarization azimuth rotation angle θ and the ellipticity angle η.

exhibits stronger optical activity. The simulated transmission and reflection spectra for the RCP and LCP waves are shown in Fig. 18(a). The effective parameters are extracted and presented in Figs. 18(b)-(c). It is observed that two resonances occurred at frequencies of 4.5 GHz and 4.9 GHz. Due to the closed resonant frequencies, the chirality parameter in the between (i.e. 4.7 GHz) is relatively large and results in a very strong optical activity. The polarization azimuth rotation angle and ellipticity angle of the transmitted wave are shown in Fig. 18(d). It is seen that at η = 0 (i.e. around 4.7 GHz), the polarization rotation angle is around 69° for 1.6-mm-thick CMM (i.e. the rotation angle is around 2752°/λ) which is much larger than the conventional U-SRRs structure.

The overall resonance behavior and mechanism of resonances of these structures is similar to the conventional conjugated gammadion and U-SRRs CMM structures. The origin of the optical activity and negative refractive index of conjugated gammadion structure can be explained based on the semi-helix chiral particle [7]. Also, the resonance behavior of the U-SRRs CMM structure is attributed to the longitudinal magnetic dipole-dipole coupling [5, 33].

V. Conclusions

We have proposed the miniaturized chiral metamaterial structures with smaller unit cells or lower resonant frequencies. According to the mechanism of resonance in CMM structures, three general ideas to miniaturize CMMs are proposed, namely, include using fractal geometries, wideband antenna designs, and meandered structures. The obtained results show that the proposed CMM structures have smaller unit cell size and moreover some of them exhibit huger pure optical activity which can be utilized as ultrathin microwave polarization rotators. The proposed miniaturized CMM structures can be scaled to other frequencies and can be utilized to improve performance of circularly polarized antennas. Also, they are simple and suitable for planar fabrication.

References

[1] I. V. Lindell, A. H. Sihvola, S. A. Tretyakov, and A. J. Viitanen, *Electromagnetic Waves in Chiral and Bi-isotropic Media*, Artech House, 1994.

[2] S. Tretyakov, I. Nefedov, A. Sihvola, S. Maslovski, and C. Simovski, "Waves and energy in chiral nihility," *Journal of Electromagnetic Waves and Applications*, vol. 17, no. 5, pp. 695-706, 2003.

[3] E. Plum, J. Zhou, J. Dong, V. A. Fedotov, T. Koschny, C. M. Soukoulis, and N. I. Zheludev, "Metamaterial with negative index due to chirality," *Phys. Rev. B* 79, 035407, 2009.

[4] J. Zhou, J. Dong, B. Wang, T. Koschny, M. Kafesaki, and C. M. Soukoulis, "Negative refractive index due to chirality," *Phys. Rev. B* 79, 121104, 2009.

[5] Z. Li, R. Zhao, T. Koschny, M. Kafesaki, and C. M. Soukoulis, "Chiral metamaterials with negative refractive index based on four "U" split ring resonators," *Appl. Phys. Lett*. 97, 081901, 2010.

[6] Z. Wu, B. Q. Zhang, S. Zhong, "A double-layer chiral metamaterial with negative index," *Journal of Electromagnetic Waves and Applications*, vol. 24, no. 7, pp. 983-992, 2010.

[7] R. Zhao, L. Zhang, J. Zhou, T. Koschny, and C. M. Soukoulis, "Conjugated gammadion chiral metamaterial with uniaxial optical activity and negative refractive index," *Phys. Rev. B* 83, 035105, 2011.

[8] Z. Li, K. B. Alici, E. Colak, E. Ozbay, "Complementary chiral metamaterials with giant optical activity and negative refractive index," *Appl. Phys. Lett*. 98, 161907, 2011.

[9] D. Zarifi, M. Soleimani, and V. Nayyeri, "Dual- and Multiband Chiral Metamaterial Structures with strong optical activity and negative refraction index," *IEEE Ant. and Wireless Propag. Lett.*, Vol. 11, 2012.

[10] A. V. Rogacheva, V. A. Fedotov, A. S. Schwanecke, and N.I. Zheludev, "Giant gyrotropy due to electromagnetic-field coupling in a bilayered chiral structure," *Phys. Rev. Lett.* 97177401, 2006.

[11] D. Kwon, P. L. Werner, and D. H. Werner, "Optical planar chiral metamaterial designs for strong circular dichroism and polarization rotation," *Opt. Express*, vol. 16, no. 16, 2008.

[12] E. Plum, V. A. Fedotov, and N. I. Zheludev, "Optical activity in extrinsically chiral metamaterial," *Appl. Phys. Lett*. 93, 191911, 2008.

[13] N. Wongkasem, A. Akyurtlu, and K. A. Marx, "Development of Chiral and Achiral Double Negative Metamaterials in the THz Regime," *Proc. SPIE* 6373, 63730Z, 2006.

[14] N. Wongkasem, A. Akyurtlu, K. A. Marx, W.D. Goodhue, J. Li, Q. Dong and E. Ada, "Lithographic Fabrication of a Novel Micron Scale Metamaterials Y-Structures-Based Chiral Metamaterial: Theoretical and Experimental Analysis of its Chiral and Negative Index of Refraction Properties in the Terahertz and Microwave Regime," *Microscopy Research and Technique*, vol.70, pp. 497-505, 2007.

[15] N. Wongkasem, A. Akyurtlu, and K. A. Marx, Q. Dong, J. Li and W.D. Goodhue, "Development of Chiral Negative Refractive Index Metamaterials for the Terahertz Frequency Regime," *IEEE Transactions on Antennas and Propagation*, vol. 55, no. 11, pp. 3052-3062, November 2007.

[16] Y. Ye, X. Li, F. Zhuang, and S. -W. Chang, "Homogeneous circular polarizers using a bilayered chiral metamaterial," *Appl. Phys. Lett.* , Vol. 99, 031111, 2011.

[17] M. Mutlu, A. E. Akosman, A. E. Serebryannikov, and E. Ozbay, "Asymmetric chiral metamaterial circular polarizer based on four U-shaped split ring resonators," *Opt. Lett.*, Vol. 36, No. 9, 2011.

[18] B. Wang, T. Koschny, and C. M. Soukoulis, "Wide-angle and polarization-independent chiral metamaterial absorber," *Phys. Rev. B*, Vol. 80, 033108, 2009.

[19] D. Zarifi, H. Oraizi, and M. Soleimani, "Improved performance of circularly polarized antenna using semi-planar chiral metamaterial covers," *Progress In Electromagnetic Research,* vol. 123, pp. 337-354, 2012.

[20] B. Wang, J. Zhou, T. Koschny, M. Kafesaki, and C. M. Soukoulis, "Chiral metamaterials: simulations and experiments," *J. Opt. A: Pure Appl. Opt*., 11:114003, 2009.

[21] R. Zhao, T. Koschny, C. M. Soukoulis, "Chiral metamaterials: retrieval of the effective parameters with and without substrate," *Opt. Express*, vol. 18, no. 14, July 2010.

[22] J. D. Jackson, *Classical Electrodynamics*, 3rd ed., Wiley, New York, 1999.

[23] G. Dolling, "Design, Fabrication and Characterization of Double-Negative Metamaterials for Photonics," Ph.D. Thesis, Dept. Phys., University of Karlsruhe, Karlsruhe, 2007.

[24] D. R. Smith, D. C. Vier, Th. Koschny, and C. M. Soukoulis, "Electromagnetic parameter retrieval from inhomogeneous metamaterials," *Phys. Rev. E* 71, 036617, 2005.

[25] W. L. Stutzman, G.A. Thiele, *Antenna Theory and Design*, 2nd ed., Wiley, New York, 1998.

[26] A. Yarive, *Optical electronics in modern communications*, 5th ed., New York: Oxford University Press, 1997.

[27] R. S. Chu, and K. M. Lee, "Analytical model of a multilayered meander-line polarizer plate with normal and oblique plane wave incident," *IEEE Trans. Antennas Propoaga*., *AP 35*, pp. 625-661, 1987.

[28] J. Hao, Y. Yuan, L. Ran, T. Jiang, J. A. Kong, C. T. Chan, and L. Zhou, "Manipulating electromagnetic waves polarizations by anisotropic metamaterials*," Phys. Rev. Lett.* 99063908, August 2007.

[29] J. Y. Chin, M. Lu, and T. J. Cui, "Metamaterial polarizers by electric-field-coupled resonators," *Appl. Phys. Lett*. vol. 93, 251903, 2008.

[30] S. R. Best, "A Comparison of The Performance Properties of The Hilbert Curve Fractal and Meander Line Monopole Antennas," *Microwave and Optical technology letters*, vol. 35, pp. 258-262, Nov. 2002.

[31] M. Reppel and J. C. Mage, "Superconducting Microstrip Bandpass Filter on $LaAlO_3$ With High Out-Of-Band Rejection", *IEEE Microwave and Guided letters*, vol. 10, pp. 180-182, May 2000.

[32] P. Jarry and J. Beneat, *Design and Realizations of Miniaturized Fractal RF and Microwave Filters*, Wiley, New Jersey, 2009.

[33] N. Liu and H. Giessen, "Three-dimensional optical metamaterials as model systems for longitudinal and transverse magnetic coupling," *Optics Express* 16, 21233, 2008.